ACS Catalysis

Research Article

Rewiring the "Push-Pull" Catalytic Machinery of a Heme Enzyme Using an Expanded Genetic Code

Mary Ortmayer, Karl Fisher, Jaswir Basran, Emmanuel M. Wolde-Michael, Derren J. Heyes, Colin Levy, Sarah L. Lovelock, J. L. Ross Anderson, Emma L. Raven, Sam Hay, Stephen E. J. Rigby, and Anthony P. Green*

Cite This: *ACS Catal.* 2020, 10, 2735−2746

Read Online

ACCESS | Metrics & More | Article Recommendations | Supporting Information

ABSTRACT: Nature employs a limited number of genetically encoded axial ligands to control diverse heme enzyme activities. Deciphering the functional significance of these ligands requires a quantitative understanding of how their electron-donating capabilities modulate the structures and reactivities of the iconic ferryl intermediates compounds I and II. However, probing these relationships experimentally has proven to be challenging as ligand substitutions accessible via conventional mutagenesis do not allow fine tuning of electron donation and typically abolish catalytic function. Here, we exploit engineered translation components to replace the histidine ligand of cytochrome *c* peroxidase (C*c*P) by a less electron-donating N_δ-methyl histidine (Me-His) with little effect on the enzyme structure. The rate of formation (k_1) and the reactivity (k_2) of compound I are unaffected by ligand substitution. In contrast, proton-coupled electron transfer to compound II (k_3) is 10-fold slower in C*c*P Me-His, providing a direct link between electron donation and compound II reactivity, which can be explained by weaker electron donation from the Me-His ligand ("the push") affording an electron-deficient ferryl oxygen with reduced proton affinity ("the pull"). The deleterious effects of the Me-His ligand can be fully compensated by introducing a W51F mutation designed to increase "the pull" by removing a hydrogen bond to the ferryl oxygen. Analogous substitutions in ascorbate peroxidase lead to similar activity trends to those observed in C*c*P, suggesting that a common mechanistic strategy is employed by enzymes using distinct electron transfer pathways. Our study highlights how noncanonical active site substitutions can be used to directly probe and deconstruct highly evolved bioinorganic mechanisms.

KEYWORDS: heme enzyme, noncanonical ligand, metal-oxo reactivity, proton-coupled electron transfer, genetic code expansion
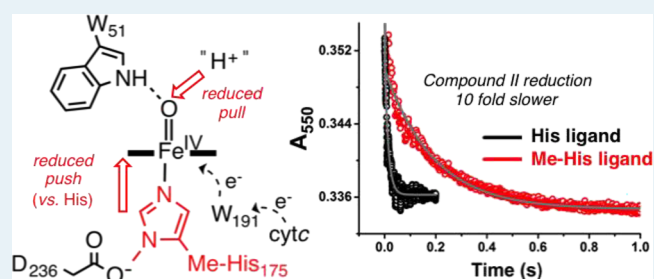
INTRODUCTION

In nature, heme enzymes catalyze a wealth of oxidative transformations. The axial ligand coordinating the heme iron varies across enzyme families and is pivotal to controlling catalytic function.[1,2] Considerable effort has been devoted to understanding relationships between proximal ligand electron donation, the structures and reactivities of iconic ferryl intermediates compound I and compound II, and overall catalytic function.[3−8] For example, the ability of cytochrome P450s and aromatic peroxygenases to functionalize unactivated C−H bonds is dependent on axial thiolate ligation. Strong electron donation ("the push") from the cysteinate ligand increases electron density on the compound I ferryl oxygen and thus enhances its reactivity with respect to C−H bond activation ("the pull").[3−7]

Heme peroxidases utilize a histidine residue as the axial ligand to the heme iron, with a hydrogen bond formed between the noncoordinating N_δ atom and a conserved aspartate residue (Figure 1a).[1,9] This interaction imparts a degree of "imidazolate-like" character onto the axial ligand,

thus increasing its electron-donating capabilities. Despite extensive theoretical and experimental studies,[10,11] the significance of this imidazolate ligand in the peroxidase catalytic mechanism remains poorly understood, presenting a missing link in our understanding of heme biochemistry. Directly probing relationships between proximal ligand electron donation and heme enzyme reactivity has proven to be extremely challenging. Ligand substitutions accessible through standard mutagenesis do not allow fine tuning of electron-donating properties and typically eliminate natural catalytic function.[12] Efforts to install a greater range of ligands have often resorted to the creation of "cavity mutants", involving replacement of large ligands by amino acids with smaller side chains (Gly or Ala) and subsequent diffusion of
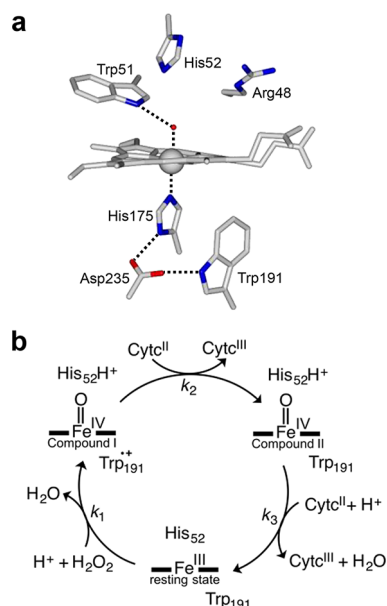
Figure 1. Structure and catalytic mechanism of cytochrome *c* peroxidase (C*c*P). (a) Active site of C*c*P (PDB code: 1ZBY).[9] The hydrogen bond between Asp235 and His175 imparts a degree of imidazolate-like character onto the axial ligand, thus increasing its electron-donating capabilities. (b) Catalytic cycle of C*c*P with its biological redox partner ferrous cytochrome *c* (cyt*c*) as an electron donor. His52 is protonated in compound I but not the resting state.[18]

exogenous ligands into the vacant coordination site. These studies have provided valuable insights into the roles of proximal heme ligands. However, the resulting ternary complexes typically fail to deliver catalysts with appreciable activity, demonstrating the importance of covalent attachment of ligands to the protein backbone.[13,14] For example, coordination of imidazole to the H175G cavity mutant of cytochrome *c* peroxidase (C*c*P) fully restores its activity with hydrogen peroxide to generate a ferryl intermediate. However, the rate of cytochrome *c* oxidation is unaffected by imidazole complexation, making it challenging to exploit this approach to quantify the impact of ligand substitutions on compound I and compound II reactivity.[14]

As a result, researchers have turned to synthetic model complexes, which offer greater versatility with respect to local metal coordination environment, to validate mechanistic hypotheses.[2,15] However, the catalytic activities of these small molecule systems are typically orders of magnitude lower than enzymes, which possess highly evolved and sophisticated catalytic mechanisms that are not replicated in synthetic complexes. The ability to selectively install a greater repertoire of metal coordinating residues into proteins could therefore offer a powerful and more direct approach to probe complex bioinorganic mechanisms. Here, we report the preparation and characterization of a functional cytochrome *c* peroxidase (C*c*P) with an N_δ-methyl histidine (Me-His) proximal ligand. In contrast to P450s where strong electron donation is linked to compound I reactivity,[3–6] we show that "electron push" from the "imidazolate-like" proximal ligand of C*c*P has little impact on compound I reactivity and instead tunes the reactivity of compound II.

RESULTS

C*c*P recruits electrons from its biological redox partner ferrous cytochrome *c* (cyt*c*) to reduce hydrogen peroxide in mitochondria.[1] The reaction mechanism is comprised of three steps (Figure 1b): (i) reaction of the resting ferric enzyme with hydrogen peroxide to generate compound I, containing an oxidized ferryl heme and a Trp191 radical cation;[16] (ii) single electron reduction of compound I by ferrous cyt*c* to generate compound II; and (iii) single electron reduction of compound II by a second equivalent of ferrous cyt*c*. Compound II reduction is coupled with proton transfer to the ferryl oxygen.[17] The distal pocket His52, which is protonated in compound I but not in the resting state,[18] is a likely source of the required proton.

To probe the influence of proximal ligand electron donation on the C*c*P catalytic mechanism, the axial His175 ligand of *S. cerevisiae* C*c*P was replaced with a noncanonical Me-His residue using an engineered pyrrolysyl-tRNA synthetase/pyrrolysyl-tRNA pair (PylRS^{Me-His}/tRNA^{Pyl}), which selectively incorporates Me-His in response to the amber UAG stop codon (Figure S1).[19] The C*c*P Me-His X-ray crystal structure, refined to a resolution of 1.90 Å (Figure S2 and Table S1), superimposes well with a previously reported C*c*P His structure[9] (Figure 2; PDB code: 1ZBY, secondary structure
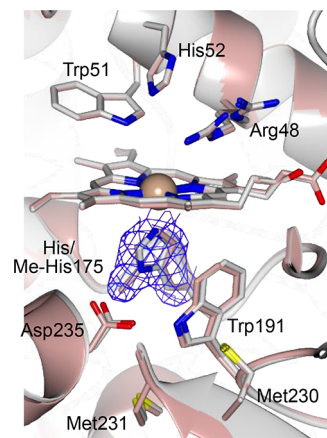

Figure 2. Structural characterization of C*c*P His and C*c*P Me-His. Overlay of C*c*P (PDB code: 1ZBY)[9] and C*c*P Me-His (PDB code: 6H08) active sites (using secondary structure superpose, RMS deviation of 0.107 Å). The C*c*P His heme cofactor and key residues are shown as atom colored sticks with gray carbons. The protein backbone is represented in cartoon format (colored in gray). The C*c*P Me-His heme cofactor and key residues are shown as atom colored sticks with pink carbons. The protein backbone is represented in cartoon format (colored in pink). The $2F_o-F_c$ electron density map corresponding to the Me-His residue is contoured at 1σ (blue mesh).

superpose, RMS deviation of 0.11 Å). Comparison of the C*c*P His and C*c*P Me-His structures demonstrates that His → Me-His constitutes a highly conservative mutation, with the geometry and environment of the heme cofactor and key active site residues well preserved in the modified enzyme. Arg48 within the distal pocket adopts two conformations as observed previously in ferric C*c*P (Figure 2).[9] Proximal ligand substitution disrupts the conserved Asp-His proximal pocket hydrogen bond responsible for increasing the electron-donating properties of His ligands in peroxidases.[1,10,11] Asp235 undergoes a minor conformational adjustment to accommodate the additional methyl substituent on the

proximal histidine ligand. The proximal Me-His adopts a similar conformation to the histidine residue in previously reported structures, thus maintaining π-stacking interactions with Trp191. Significantly, the environment surrounding the redox-active Trp191 residue is fully conserved in the CcP Me-His structure, including the hydrogen-bonding interaction with Asp235 and interactions with nearby Met230 and Met231 residues that are important for the stability of the compound I Trp191 radical cation.[1] This contrasts with previous attempts to modulate proximal ligand electron donation in CcP through mutation of Asp235, which resulted in dramatic reorientation of the Trp191 residue.[20]

Introduction of a proximal Me-His ligand resulted in a 22-fold reduction in k_{cat} for the oxidation of ferrous cytc from horse heart (pH 6.0, 25 °C) ($k_{cat} = 805 \pm 25$ s^{-1} for CcP His, $k_{cat} = 38 \pm 5$ s^{-1} for CcP Me-His) with only modest changes in K_M (Figure 3a and Table 1). Despite the reduction in k_{cat}, CcP
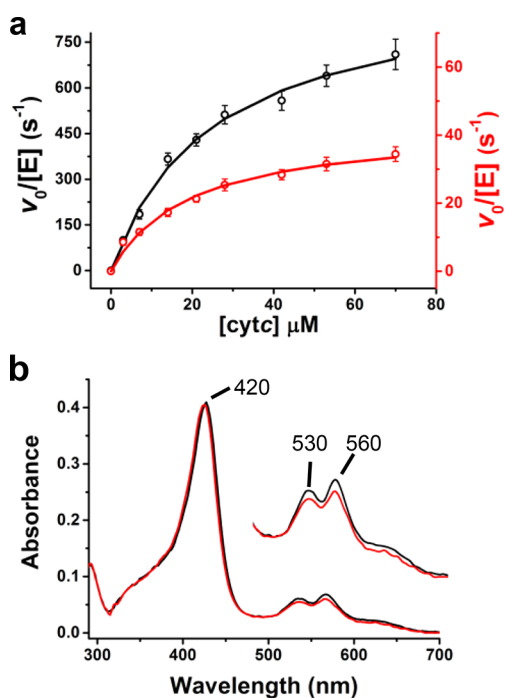

Figure 3. Kinetic and spectroscopic characterization of CcP His and CcP Me-His. (a) Michaelis−Menten plots of cytc oxidation by CcP His (black, $k_{cat} = 805 \pm 25$ s^{-1}, $K_M^{cytc} = 18 \pm 3$ μM) and CcP Me-His (red, $k_{cat} = 38 \pm 5$ s^{-1}, $K_M^{cytc} = 17 \pm 2$ μM). Measurements at pH 6, 25 °C, error bars are SEM, $n = 3$. (b) Overlay of the UV−vis spectra of the compound I states of CcP (black) and CcP Me-His (red).

Table 1. Cytc Oxidation Kinetic Parameters for CcP His, CcP Me-His, and Their W51F Variants[a]

variant	k_{cat} (s^{-1})	K_M (μM)
CcP	805 ± 25 (590 ± 21)[b]	18 ± 3 (16 ± 2)
CcP Me-His	38 ± 5 (25 ± 4)	17 ± 2 (18 ± 2)
CcP W191F	ND[c]	
CcP W191F Me-His	ND	
CcP W51F	2350 ± 100	14 ± 2
CcP W51F Me-His	1170 ± 30	18 ± 2

[a]All measurements were carried out at 25 °C in potassium phosphate (50 mM) at pH 6.0. [b]Values in parentheses correspond to measurements in D_2O. [c]ND: no activity detected above background.

Me-His is able to oxidize >10,000 equivalents of ferrous cytc with no evidence of enzyme deactivation. Mutation of the proximal pocket Trp191 residue to phenylalanine in CcP Me-His and CcP His eliminates catalytic activity, demonstrating that this redox-active residue retains an essential role in the catalytic function of the modified enzyme. In contrast to the substantially reduced k_{cat} observed with the biological redox partner ferrous cytc, proximal ligand substitution has minimal effects on the kinetics of guaiacol (ortho-methoxyphenol) oxidation (Figure S3b), suggesting that the noncanonical active site modification specifically perturbs long-range electron transfer from cytc mediated through Trp191.

Replacement of the proximal His ligand by Me-His increases the midpoint reduction potential for the heme Fe^{III}/Fe^{II} couple by +35 ± 1 mV (Figure S4), consistent with reduced electron donation from the proximal ligand. This increased potential can be attributed to loss of a hydrogen bond between the proximal ligand and Asp235. Despite this reduced electron donation, the UV−vis spectra of CcP Me-His in the ferric state and compound I and compound II states are highly similar to the corresponding spectra of the wild-type enzyme (Figure 3b and Figures S5 and S6). The compound I and compound II states of CcP are not distinguishable by UV−vis spectroscopy, with spectral features consistent with a neutral ferryl heme (Soret maxima at 420 nm and associated Q bands at 530 and 560 nm).

In CcP His, the second oxidizing equivalent of compound I is stored as a stable Trp191 radical cation, which is an essential intermediate along the electron transfer pathway from ferrous cytc.[16] To confirm the identity of the protein-based radical cation in CcP Me-His, compound I was characterized by X-band continuous wave electron paramagnetic resonance (EPR) spectroscopy. CcP His compound I has previously been shown to produce a distinctive EPR signal at 10 K or below that arises from a distribution of scalar magnetic or exchange coupling (J) values between the S = 1 ferryl (FeIV=O) heme and the S = 1/2 tryptophan cation radical spin systems.[16,21] That EPR signal was reproduced in our experiments (Figure 4), having a shoulder at $g = 2.04$ and crossing point at $g = 2.00$ at 6 K. Global replacement of tryptophan residues in CcP His with L-tryptophan-(indole-d_5) gave rise to changes in the EPR signal arising from hyperfine coupling to the C$_\beta$-protons that are now resolved in the absence of the hyperfine contributions from the indole ring protons. Additionally, deuteration leads to a slight narrowing and shift of the shoulder at $g = 2.04$ due to a reduction in unresolved proton hyperfine coupling. These effects confirm the contribution made by the tryptophan cation radical to the compound I signal. This signal is present at 94−97% of heme concentration in the CcP His preparations as judged by double integration at nonsaturating powers against Cu(II)−EDTA standards. The 6 K compound I EPR signal associated with CcP Me-His (present at 83−86% of heme concentration) lacks the shoulder at $g = 2.04$; however, L-tryptophan-(indole-d_5) substitution gives rise to similar effects to those observed in CcP His, though naturally less dramatic on the narrower CcP Me-His signal. Spectra of CcP Me-His compound I bearing the W191F mutation are consistent with the formation of relatively low yielding (~15% of heme concentration) adventitious tyrosine radicals remote from the heme, as previously observed in the W191F and W191G variants of CcP His.[22,23] Therefore, despite exhibiting an EPR signal line shape different from that of CcP His, CcP Me-His forms a compound I characterized by a ferryl heme exchange
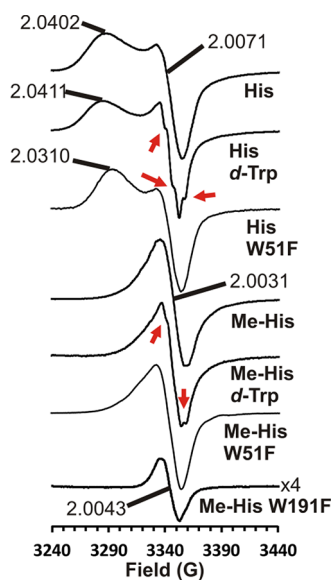
Figure 4. X-band continuous wave EPR spectra of the compound I state of CcP His and CcP Me-His with and without the additional W51F mutation. EPR spectra recorded at 6 K showing the effect of tryptophan-(indole-d_5) on the spectra and a comparison with the CcP Me-His W191F variant; g values are marked, and red arrows indicate partially resolved hyperfine splitting.

coupled to a Trp191 radical cation, with the differences in line shape being attributable to a change in that ferromagnetic coupling. Houseman et al.[21] state in their original determination of the value(s) of J for CcP His that "given the tiny energies associated with the heme-radical spin coupling, it is hardly surprising that the EPR spectrum of compound I should be exquisitely sensitive to small perturbations in the protein's surroundings."

Rate constants for the three elementary steps (k_1, k_2, and k_3; Figure 5a) in the catalytic cycle of CcP His and CcP Me-His were determined at 4 °C using established stopped-flow techniques.[24] Introduction of the less electron-donating Me-His ligand has a negligible impact on the rate constant for compound I formation ($k_1 = (3.5 \pm 0.7) \times 10^7$ M^{-1} s^{-1} for CcP and $k_1 = (3.3 \pm 0.4) \times 10^7$ M^{-1} s^{-1} for CcP Me-His; Figure 5b and Figure S7a−d,i). Likewise, the rate constant for compound I reduction is unaffected by proximal ligand substitution ($k_2 = (1.16 \pm 0.12) \times 10^8$ M^{-1} s^{-1} in CcP His and $k_2 = (1.14 \pm 0.25) \times 10^8$ M^{-1} s^{-1} in CcP Me-His; Figure 5c and Figure S7l), demonstrating that the natural electron transfer pathway from ferrous cytc to Trp191 is maintained in the modified enzyme and that the redox potential of Trp191 has not been significantly altered by axial ligand substitution. In contrast, compound II reduction is 10-fold slower in CcP Me-His ($k_3 = (2.6 \pm 0.1) \times 10^5$ M^{-1} s^{-1} vs $(2.7 \pm 0.2) \times 10^6$ M^{-1} s^{-1} for CcP His; Figure 5d and Figure S7e−h,j). This 10-
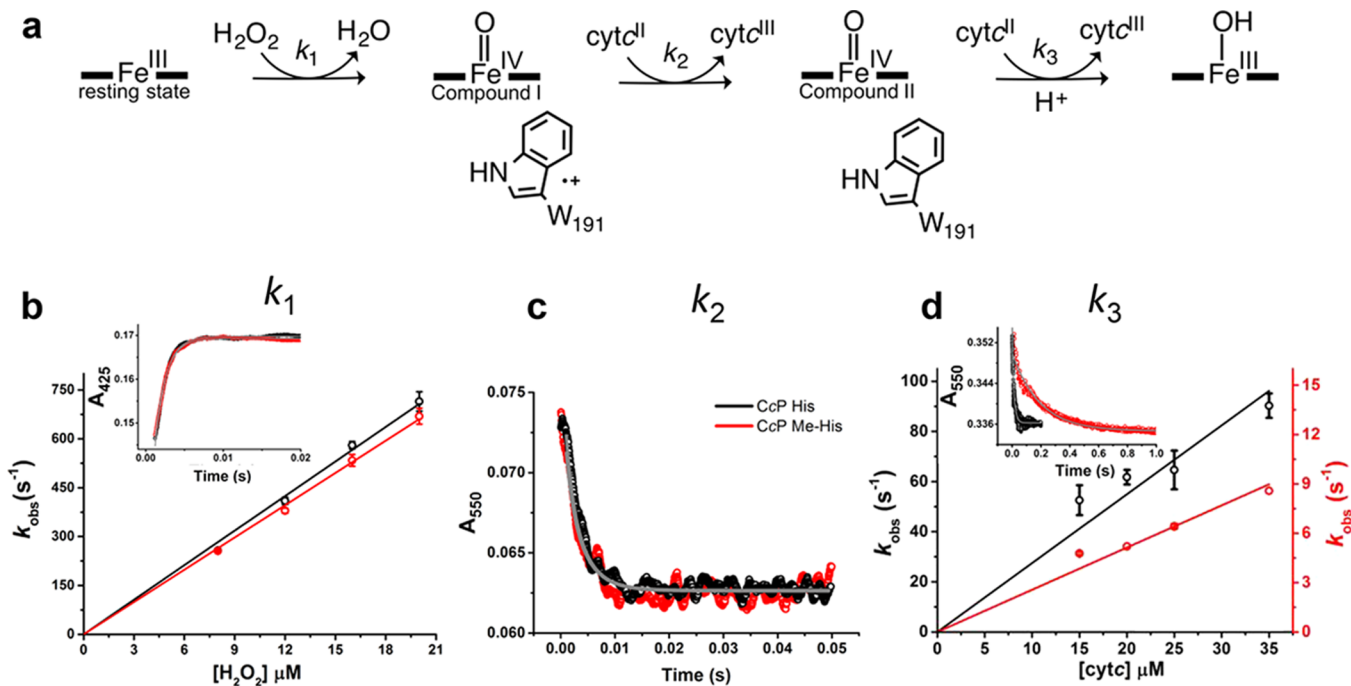

Figure 5. Pre-steady-state kinetic characterization of CcP His and CcP Me-His. (a) Catalytic mechanism of CcP. (b) Observed rate constants for compound I formation at varying H$_2$O$_2$ concentrations. Representative kinetic traces at 20 μM H$_2$O$_2$ are shown (inset). A linear fit of k_{obs} versus [H$_2$O$_2$] was used to derive bimolecular rate constants of $k_1 = (3.5 \pm 0.7) \times 10^7$ M^{-1} s^{-1} for CcP His (black) and $k_1 = (3.3 \pm 0.4) \times 10^7$ M^{-1} s^{-1} for CcP Me-His (red). Error bars represent SD, $n = 3$. (c) Averaged kinetic traces ($n = 3$) for compound I reduction for both CcP His (black) and CcP Me-His (red). Conditions: CcP His/CcP Me-His (4 μM), H$_2$O$_2$ (8 μM), and a delay time of 1 s before reaction with cytc (1.5 μM) (post-mixing concentrations). Reactions were monitored by reduction in absorbance at 550 nm due to oxidation of ferrous cytc. These data are fitted to an integrated second-order rate equation (gray lines) to derive an apparent intrinsic rate constants of $k_2 = (1.16 \pm 0.12) \times 10^8$ M^{-1} s^{-1} in CcP His and $k_2 = (1.14 \pm 0.25) \times 10^8$ M^{-1} s^{-1} in CcP Me-His. The instrument dead time for the determination of k_2 is <1.5 ms. (d) Observed rate constants for compound II reduction at varying cytc concentrations. Representative kinetic traces at 35 μM are shown (inset), and all data were fitted to $A_{550} = A_0 + \Delta A(e^{-k_2[cytc]_0 t} + e^{-k_{obs}t})$ with k_2 fixed to the value determined above. A linear fit of k_{obs} versus [cytc] was used to derive bimolecular rate constants for CcP His (black, $k_3 = (2.7 \pm 0.2) \times 10^6$ M^{-1} s^{-1}) and CcP Me-His (red, $k_3 = (2.6 \pm 0.1 \times 10^5$ M^{-1} s^{-1}). Error bars are SD ($n = 2$ for CcP Me-His; $n = 3-5$ for CcP His). All measurements are at pH 6, 4 °C.
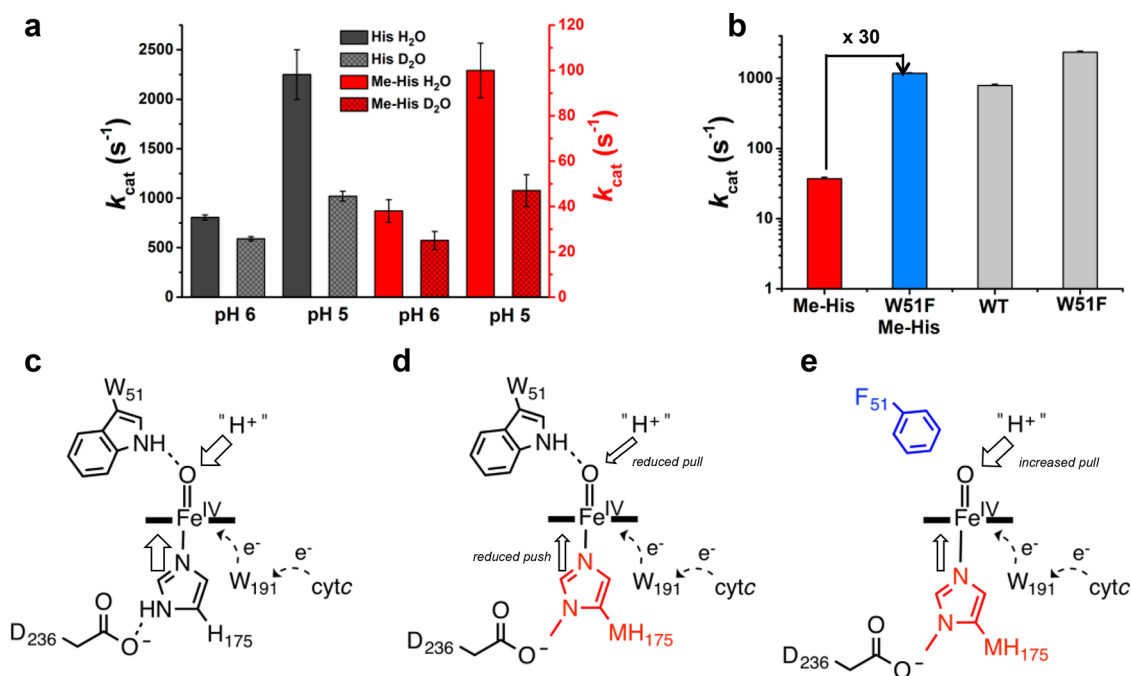
Figure 6. Solvent kinetic isotope effects and the role of Trp51 in controlling compound II proton affinity and reactivity. (a) Bar chart showing the solvent kinetic isotope effect on k_{cat} for cyt$c$ oxidation by CcP His and CcP Me-His at pH/pD = 6 and pH/pD = 5. CcP His: KSIE = 1.4 (pH/pD = 6) and KSIE = 2.2 (pH/pD = 5). CcP Me-His: KSIE = 1.5 (pH/pD = 6) and KSIE = 2.1 (pH/pD = 5). (b) Bar chart showing the kinetics (k_{cat}) of cyt$c$ oxidation by CcP His, CcP Me-His, and their W51F variants. (c–e) Schemes for proton-coupled compound II reduction in (c) CcP His, (d) CcP Me-His, and (e) CcP Me-His W51F, highlighting the importance of axial ligand electron donation (the "push") and hydrogen-bonding interactions with Trp51 in controlling the proton affinity of the ferryl oxygen (the "pull"). The proton ("H") is likely transferred from His52 via an ordered water molecule.[17]

fold reduction in k_3 also correlates with a comparable reduction in k_{cat} in steady-state assays at 4 °C (k_{cat} = 235 ± 35 s^{-1} for CcP His and k_{cat} = 22 ± 5 s^{-1} for CcP Me-His; Figure S3c,d).

The relationship between axial ligand substitution and compound II reactivity cannot be rationalized through consideration of the driving force for electron transfer, which is greater in CcP Me-His due to the increase in heme redox potential. However, differences in electronic coupling between Trp191 and the heme center upon ligand substitution could potentially give rise to reduced electron transfer rates due to modulation of the electron transfer pathway. Alternatively, compound II reduction in heme peroxidases is thought to be coupled to proton transfer to the ferryl oxygen, with significant solvent kinetic isotope effects (KSIEs) reported previously for ascorbate peroxidase and *Leishmania* peroxidase (LmP).[25,17] The less electron-donating Me-His ligand could give rise to a less basic ferryl oxygen and consequently perturb proton-coupled electron transfer to the ferryl heme (Figure 6c,d). The pK_a of metal-oxo bonds is known to be exquisitely sensitive to the electron-donating capabilities of ancillary ligands.[26]

To distinguish between these two mechanistic hypotheses, we performed activity assays in buffered H$_2$O and D$_2$O. Kinetic characterization of CcP His and CcP Me-His (pH/pD 6.0) revealed a KSIE of 1.4 and 1.5, respectively, with no effect on K_M in either variant (Figure 6a). We also investigated the influence of pH/pD on CcP His and CcP Me-His activity. For both variants, initial reaction velocities increase with decreasing pH/pD between 6 and 5 (Figure S8a,b). The increased reaction rates also correlate with increasing KSIEs across the series, with values of 2.2 and 2.1 determined for CcP His and CcP Me-His, respectively, at pH/pD = 5 (Figure 6a). These

data demonstrate that proton transfer is involved in rate-limiting compound II reduction in CcP His and CcP Me-His and suggest that the observed electron donation–compound II reactivity trend can be explained by considering the proton affinity ("the pull") of the ferryl oxygen (Figure 6c,d).

We therefore considered alternative factors that are likely to govern the pK_a of compound II. The N–H group of Trp51 forms a hydrogen bond to the ferryl oxygen,[18] an interaction that can be expected to withdraw electron density from the Fe(IV)=O unit. We reasoned that deletion of this hydrogen bond using a W51F mutation in CcP His and Me-His would provide a means of increasing the pK_a of the ferryl oxygen without causing significant disruption of the electron transfer pathway from Trp191 to the heme iron. Indeed, EPR spectra at 6 K of compound I generated in W51F CcP and W51F CcP Me-His demonstrate formation of a ferryl heme:Trp191 exchange-coupled species (Figure 4). Consistent with a previous study,[27] a W51F mutation in CcP His leads to a 3-fold increase in cyt$c$ oxidation activity (k_{cat} = 2350 ± 100 s^{-1}). This activity has been previously been shown to be strictly dependent on the presence of Trp191, demonstrating that the natural electron transfer pathway is maintained in the W51F mutant.[28] The W51F substitution in CcP Me-His leads to a more dramatic 32-fold increase in k_{cat} (1170 ± 30 s^{-1}, ferrous cyt$c$ oxidation) (Figure 6b,e and Figure S3f). Thus, the deleterious effects of reduced electron donation from the Me-His axial ligand can be fully compensated by removing a single hydrogen-bonding interaction to the ferryl oxygen (Figure 6d,e) to afford a variant (W51F CcP Me-His) with catalytic features reminiscent of the wild-type enzyme, further underscoring the importance of Fe(IV)=O pK_a in governing compound II reactivity.

A strongly electron-donating "imidazolate-like" axial ligand is a conserved feature across the heme peroxidase family. To investigate whether this ligand plays an important role in tuning Fe(IV)=O pK_a and catalytic activity in family members other than CcP, we elected to reengineer the heme coordination environment of ascorbate peroxidase (APX). We have previously shown that introducing a Me-His ligand into an evolved ascorbate peroxidase (APX2) has negligible effects on the efficiency of guaiacol oxidation but increases the robustness of the enzyme toward irreversible deactivation during catalysis.[29] The active site structure and overall catalytic mechanism of APX is highly similar to that of CcP. Compound II reduction is rate-limiting,[30] and electron transfer from ascorbate is thought to be coupled with proton transfer to the ferryl oxygen.[25] However, unlike CcP, the proximal pocket Trp179 of APX does not participate in redox chemistry, and electron transfer to the heme occurs directly from the small molecule substrate ascorbate bound at the γ-heme edge (Figure 7).[31] Consequently, we reasoned that axial ligand
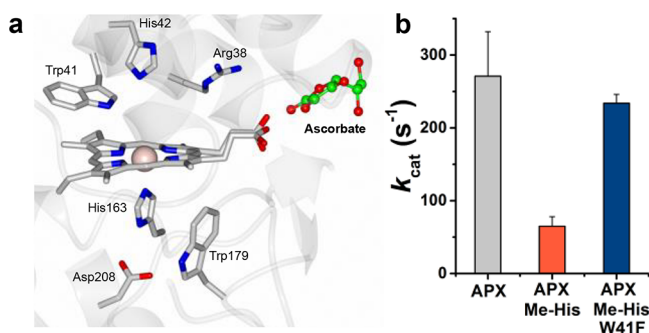

Figure 7. Kinetic characterization of ascorbate peroxidase (APX) and key active site mutants. (a) Active site of APX showing the substrate ascorbate bound at the γ-heme edge (PDB code: 1OAF).[31] (b) Bar chart showing the kinetics (k_{cat}) of ascorbate oxidation by APX His, APX Me-His, and APX Me-His W51F. Measurements are recorded at 25 °C in phosphate buffer (50 mM, pH 6).

substitution in APX would provide a means of tuning Fe(IV)=O pK_a without causing significant perturbations to the pathway of electron transfer from the substrate to the heme center. His → Me-His ligand substitution in APX leads to a substantial reduction in k_{cat} for ascorbate oxidation (pH 6.0, 25 °C) (k_{cat} = 270 ± 71 s^{-1} for APX His and k_{cat} = 66 ± 13 s^{-1} for APX Me-His) with negligible changes in K_M (Figure 7 and Figure S9). We have previously shown that this substitution causes only minor structural changes similar to those observed in CcP.[29] Significantly, the activity of APX Me-His can be restored to wild-type levels by introducing a W41F substitution designed to increase Fe(IV)=O pK_a (k_{cat} = 234 ± 12 s^{-1} for APX Me-His W41F). These activity trends mirror the trends observed in CcP (Figure 6b), suggesting that a common mechanistic strategy is employed by enzymes using distinct electron transfer pathways. Combined, these data provide further evidence of the relationships between Fe(IV)=O basicity and reactivity.

■ DISCUSSION

The ability to expand upon nature's genetic code to selectively install noncanonical ligands into proteins provides exciting new opportunities to directly probe metalloenzyme mechanisms.[32] For example, selenocysteine has proven to be a valuable

surrogate for axial heme thiolate ligands.[33−35] We have recently demonstrated that introduction of a Me-His proximal ligand into an evolved ascorbate peroxidase (APX2)[29] and into the oxygen binding protein myoglobin[36] improves catalytic performance towards nonbiological oxidations of model phenolic substrates.

An expanded genetic code has now allowed us to elucidate the functional significance of the "imidazolate-like" axial ligand of a heme peroxidase. Replacement of the proximal histidine ligand of CcP by Me-His provides a means of disrupting the hydrogen bond between Asp235 and the axial histidine while preserving catalytic function and, crucially, the environment surrounding the key redox-active Trp191 residue. This contrasts with previous attempts to modulate proximal ligand electron donation through mutation of Asp235, which resulted in dramatic reorientation of the Trp191 residue and complete loss of activity.[20] Surprisingly, replacement of the His ligand by Gln has previously been shown to have little effect on the rate of cyt$c$ oxidation.[37] However, whilst a W191F mutation in CcP His or CcP Me-His abolishes activity, the CcP H175Q W191F double mutant maintains high levels of activity. The H175Q mutation thus appears to open up alternative electron pathways from cyt$c$ to the ferryl heme of CcP that are not utilized in the natural catalytic cycle.

The availability of a functional CcP with a modified axial ligand allowed us to directly probe and quantify the impact of altered ligand electron donation on the reactivity of the iconic ferryl intermediates compound I and compound II. Replacement of the proximal histidine ligand of CcP by a less electron-donating Me-His has little effect on the rate of formation of compound I. This contrasts with the substantial increase in rate constant for the formation of ferryl intermediates observed upon His → Me-His ligand substitution in myoglobin,[36] an oxygen binding protein that has served as a valuable model system to probe heme enzyme structure−function relationships. Introduction of the Me-His ligand into CcP also has negligible effects on the rate constant for compound I reduction, demonstrating that the natural electron transfer pathway from ferrous cyt$c$ to Trp191 is maintained in the modified enzyme. In contrast, compound II reduction is 10-fold slower in CcP Me-His, providing a direct link between axial ligand electron donation and compound II reactivity. Our combined data present a compelling body of evidence in support of Fe(IV)=O pK_a being a key determinant of compound II reactivity in heme peroxidases, with reduced electron donation from the noncanonical Me-His ligand ("the push") affording an electron-deficient ferryl oxygen with decreased proton affinity ("the pull") compared with the wild-type enzyme. The deleterious effects of the Me-His ligand can be fully compensated by introducing a W51F mutation designed to increase "the pull" by removing a hydrogen bond to the ferryl oxygen. This ability to rationally rewire the catalytic machinery of CcP NMH provides strong evidence to support our mechanistic interpretations. The W51F mutation in CcP His has previously been shown to increase the reactivity of the ferryl heme center. However, the molecular origins of this increased reactivity are not well defined. For example, it has been suggested that introduction of the smaller Phe residue provides more space and flexibility in the heme pocket that could give rise to the observed activity changes.[38] Elsewhere, the increased rate of compound II reduction has been ascribed to an increase in activation entropy, which the authors suggest may arise due to a more facile release of the ferryl oxygen atom

as water.[39] We instead propose that the W51F substitution serves to facilitate proton transfer to the ferryl oxygen, which is required prior to the dissociation of water. This interpretation is consistent with the large increase in cyt*c* oxidation activity due to W51F mutation in C*c*P Me-His and the substantial kinetic solvent isotope effects observed for C*c*P His and C*c*P Me-His.

In summary, this study sheds light on long-standing questions in heme biochemistry and advances our fundamental understanding of biological electron transfer events. Proton-coupled electron transfers and related H atom transfers to high-valent metal-oxo intermediates are thought to be ubiquitous in biological systems and have been implicated as key steps in the catalytic mechanisms of several histidine ligated metalloenzymes.[40,41] Our methodology is thus expected to provide a versatile strategy to deconstruct these complex and sophisticated bioinorganic mechanisms and can be extended to probe and tune the reactivities of isoelectronic heme carbene and nitrene intermediates.[42] Such insights into the subtle interplay between the active site structure and catalytic activity will be critical for future efforts to rationally create functional metalloenzymes.

■ EXPERIMENTAL PROCEDURES

Materials. All materials were obtained from Sigma-Aldrich unless otherwise stated. Oligonucleotides were synthesized by MWG Eurofins (Ebersberg, Germany). Ferric cyt*c* from horse heart was obtained from Sigma-Aldrich and used throughout the study.

Construction of pET-11a_CcP, pET-11a_CcP_Me-His, and Their Variants. The gene encoding cytochrome *c* peroxidase (Ccp1p from the *S. cerevisiae* YJM1444 genome) was PCR amplified from plasmid pLeics03CCP39 (a modified version of an original C*c*P clone)[43] using Phusion High-Fidelity DNA polymerase (New England BioLabs, UK). Primers contained a N-terminal His tag and complimentary sequences to allow insertion of the PCR product into pET-11a plasmid using In-Fusion Advantage PCR Cloning via *Nde*I and *Bam*HI restriction sites, yielding pET-11a_C*c*P. The His175Me-His mutation was introduced into the pET-11a_C*c*P by replacing the His175 codon with a TAG stop codon. Site-directed mutagenesis using the Q5 Site-Directed Mutagenesis Kit (New England BioLabs, UK) of pET-11a_C*c*P yielded pET-11a_C*c*P_Me-His. W191F and W51F mutations were introduced into pET-11a_C*c*P and pET-11a_C*c*P_Me-His using the Q5 Site-Directed Mutagenesis Kit. Correct DNA sequences were confirmed by DNA sequencing (MWG Eurofins).

Construction of pET-29b_APX, pET-29b_APX _Me-His. An engineered monomeric soybean ascorbate peroxidase (APX) containing K14D, E112K, and A134P mutations was used throughout this study.[44] We have previously created the p29b_APX2 and p29b_APX2_Me-His constructs required for the production of APX W41F and APX Me-His W41F, respectively.[29] To create pET-29b_APX and pET-29b_APX Me-His, an F41W mutation was introduced into p29b_APX2 and p29b_APX2_Me-His using assembly PCR followed by restriction cloning using *Nde*I and *Xho*I sites.

Protein Production and Purification. For expression of C*c*P and its variants, BL21(DE3) *E. coli* were transformed with pET-11a_C*c*P, pET-11a_C*c*P_W51F, and pET-11a_C*c*P_W191F, and the cells were plated onto LB agar (Formedium, Norfolk, UK) plates containing 50 μg/mL

ampicillin. For expression of APX, BL21(DE3) *E. coli* was transformed with pET-29b_APX, and the cells were plated onto LB agar (Formedium, Norfolk, UK) plates containing 50 μg/mL kanamycin. A single colony of freshly transformed cells was cultured for 18 h in 10 mL of LB medium containing 50 μg/mL ampicillin or kanamycin (for C*c*P or APX, respectively). Four milliliters of the culture was used to inoculate 400 mL of 2xYT medium (Formedium, Norfolk, UK) supplemented with 1 mM δ-aminolevulinic acid and 50 μg/mL of the appropriate antibiotic.

The culture was incubated for ∼2 h at 37 °C with shaking at 180 rpm. When the OD_{600} of the culture reached ∼0.5, IPTG was added to a final concentration of 100 μM. The induced cultures were incubated for ∼20 h at 25 °C, and the cells were subsequently harvested by centrifugation at 7000*g* for 10 min.

For expression of C*c*P Me-His and its variants, BL21(DE3) *E. coli* were co-transformed with pET-11a_C*c*P_Me-His/ pET-11a_C*c*P_Me-His_W191F/pET-11a_C*c*P_Me-His_W51F and pEVOL_PylRSMe-His,[29] and the cells were plated onto LB agar plates containing 50 μg/mL ampicillin and 34 μg/mL chloramphenicol. For expression of APX Me-His and APX Me-His W41F, BL21(DE3) *E. coli* were transformed with pET-29b_APX Me-His and p29b_APX2_Me-His, and the cells were plated onto LB agar (Formedium, Norfolk, UK) plates containing 50 μg/mL kanamycin and 34 μg/mL chloramphenicol. A single colony of freshly transformed cells was cultured for 18 h in 10 mL of LB medium containing 50 μg/mL ampicillin or kanamycin (for C*c*P or APX, respectively) and 34 μg/mL chloramphenicol. Four milliliters of the culture was used to inoculate 400 mL of 2xYT medium supplemented with 1 mM δ-aminolevulinic acid, 10 mM H-His(3-Me)-OH (Me-His) (Bachem, Saint Helens, UK), 50 μg/mL of the appropriate antibiotic, and 34 μg/mL chloramphenicol. The culture was incubated for ∼2.5 h at 37 °C with shaking at 180 rpm. When the OD_{600} of the culture reached ∼0.5, IPTG and arabinose were added to a final concentration of 100 μM and 0.05%, respectively. The induced cultures were incubated for ∼20 h at 25 °C, and the cells were subsequently harvested by centrifugation at 7000*g* for 10 min.

The pelleted bacterial cells were suspended in phosphate buffer (50 mM KPi, 300 mM NaCl, 10 mM imidazole, pH 7.5) supplemented with lysozyme (1 mg/mL), DNase (0.1 U/mL), and a Complete EDTA free protease inhibitor cocktail tablet (Roche) and subjected to sonication (13 mm probe, 15 min, 20 s on, 40 s off, 40% amplitude). Cell lysates were centrifuged at 27,000*g* for 30 min, and the supernatants were subjected to affinity chromatography using Ni-NTA Agarose (Qiagen, West Sussex, UK). His-tagged C*c*P and APX variants were eluted by 50 mM KPi, 300 mM NaCl, pH 7.5 buffer containing 300 mM imidazole. The purified protein was desalted using a 10DG desalting column (Bio-Rad, Hertfordshire, UK) into 50 mM KPi, pH 6 buffer. To maximize heme occupancy, variants were reconstituted with hemin chloride. Cell suspensions were mixed with 0.5 mM hemin chloride (50 mM stock solution in 10 mM NaOH) for 30 min at room temperature (RT) and filtered through a 0.45 micron membrane. The C*c*P and C*c*P Me-His variants were then subjected to anion exchange chromatography with 50 mM KPi, pH 6 buffer using a ResourceTM Q column on an AKTA Fast Protein Liquid Chromatography (FPLC) system (both from GE Healthcare, Buckinghamshire, UK). Proteins were eluted by a linear gradient of NaCl in the concentration range of 0−500 mM, and the eluate was collected in 2 mL fractions. The purest

fractions were selected after spectral analysis, pooled, and concentrated using Vivaspin 20 centrifugal concentrators (Generon, Berkshire, UK) with a 10 kDa molecular weight cutoff membrane. The protein was aliquoted, flash-frozen in liquid nitrogen, and stored at −80 °C. The concentrations of CcP and APX proteins were determined assuming an extinction coefficient of 101 mM^{-1} cm^{-1} at 408 nm and 128 mM^{-1} cm^{-1} at 405 nm, respectively.[2,29] The heme occupancies of purified proteins and their variants are comparable, with similar Rz (A410/A280) values of ~1.5.

Production of CcP and CcP Me-His Containing L-Tryptophan-(Indole-d_5). For expression of L-tryptophan-(indole-d_5) CcP (d-Trp CcP) and L-tryptophan-(indole-d_5) CcP Me-His (d-Trp CcP Me-His), BL21(DE3) E. coli were transformed with pET-11a_CcP or pET-11a_CcP_Me-His and pEVOL_PylRSMe-His, respectively, and single colonies were cultured for 18 h in 10 mL of LB medium containing the appropriate antibiotics. Two milliliters of the culture was used to inoculate 200 mL of M9 minimal medium containing 33.7 mM Na$_2$HPO4, 22.0 mM KH$_2$PO$_4$, 8.55 mM NaCl, 9.35 mM NH$_4$Cl, 0.4% glucose, 1 mM MgSO$_4$, 0.3 mM CaCl$_2$, 1 μg/L biotin and 1 μg/L thiamin, 1 x trace elements solution (100 x trace element solution, 13.4 mM EDTA, 3.1 mM FeCl$_3$·6H$_2$O, 0.62 mM ZnCl$_2$, 76 μM CuCl$_2$·2H$_2$O, 42 μM CoCl$_2$·2H$_2$O, 162 μM H$_3$BO$_3$, 8.1 μM MnCl$_2$·4H$_2$O), 0.08% Trp DROP OUT Complete Supplement Mixture (Formedium), and 10 mM L-tryptophan-(indole-d_5). Cultures were induced and pelleted as above, and the proteins were purified as described above. Complete replacement of all tryptophans with L-tryptophan-(indole-d_5) was confirmed by mass spectrometry (MS) (Figure S1).

MS Analysis. Purified protein samples were buffer-exchanged into 0.1% acetic acid using a 10K MWCO Vivaspin (Sartorius) and diluted to a final concentration of 0.5 mg ml^{-1}. MS was performed using a 1200 series Agilent LC, 5 μL injection into 5% acetonitrile (with 0.1% formic acid), and desalted inline for 1 min. Protein was eluted over 1 min using 95% acetonitrile with 5% water. The resulting multiply charged spectrum was analyzed using an Agilent QTOF 6510 and deconvoluted using Agilent MassHunter Software. All data are presented in Figure S1.

Crystallization, Refinement, and Model Building. CcP Me-His was crystallized at 50 mg ml^{-1} in 50 mM KPi, pH 6 buffer. Initial crystallization conditions were identified using the JCSG+ matrix screen (Molecular dimensions). Crystals suitable for diffraction experiments were obtained by sitting drop vapor diffusion at 4 °C in 400 nL drops containing equal volumes of protein and a solution containing 5 mM cobalt(II) chloride hexahydrate, 5 mM cadmium chloride hemi-(pentahydrate), 5 mM magnesium chloride hexahydrate, 5 mM nickel(II) chloride hexahydrate, 0.1 M HEPES (pH 7.5), and 12% (w/v) PEG 3350. The crystals were cryoprotected by the addition of 10% PEG 200 to the mother liquor and flash-cooled in liquid nitrogen. Data were collected on beamline IO4-1 (wavelength, 0.9159 Å) at the Diamond Light Source Facility and reduced and scaled with the X-ray Detector Software suite (XDS37). The CcP Me-His crystal structure was determined by molecular replacement using the PHASER program in the CCP4 suite[45] using the WT CcP structure as the starting model (PDB code: 2CYP). The CcP Me-His model was completed by iterative cycles of manual model building and real-space refinement using the program Coot and crystallographic refinement using Refmac. The processing

and final refinement statistics are presented in Table S1. Coordinates and structure factors have been deposited in the Protein Data Bank under accession number 6H08.

Spectroscopic Characterization of CcP and CcP Me-His Variants. UV−vis absorption analysis was carried out on a Cary 50Bio UV−vis spectrophotometer (Varian, CA, USA) using a 1 cm path length quartz cuvette, recording spectra between 250 and 700 nm and typically with CcP at 4 μM in 50 mM KPi, pH 6 buffer (see Figure S5).

Steady-State Enzyme Kinetic Assays. Steady-state enzyme assays were carried out on a Cary 50Bio UV−vis spectrophotometer (Varian, CA, USA) in 50 mM KPi pH 6 using a 1 mL quartz cuvette (1 cm path length). For cytc oxidation assays CcP, CcP W51F, CcP Me-His, and CcP W51F Me-His variants were diluted to 1.0 μM on the basis of the heme absorption. CytcII was prepared by reduction with dithionite, and the excess reductant was removed with a 10DG desalting column. The concentration of cytcII was calculated using the extinction coefficient ε_{550} = 27.7 mM^{-1} cm^{-1}.[44] At each concentration of cytc (0−100 μM), CcP, CcP W51F, CcP Me-His, and CcP W51F Me-His variants were diluted to 1, 1, 10, and 1 nM, respectively. H$_2$O$_2$ (100 μM) was added to initiate the reaction, and the rate of change in absorbance at 550 nm was monitored over 1 min at 25 °C. The difference in absorptivity of cytcII and cytcIII was calculated using $\Delta\varepsilon_{550}$ = 19.5 mM^{-1} cm^{-1}.[46] Reactions were performed in triplicate (at RT and 4 °C) to produce a mean rate calculated as moles of cytcII oxidized per mol CcP per second. These data were plotted against the relevant cytcII concentration and fitted using the Michaelis−Menten hyperbolic function within Origin software. Reported values are corrected for background cytc oxidation in the absence of enzyme. For CcP His W191F and CcP W191F Me-His at 50 nM, no activity was observed above background. For ascorbate oxidation assays, APX, APX Me-His, and APX Me-His W41F variants were diluted to 1 μM on the basis of the heme absorption. At each concentration of ascorbate (0−1100 mM), APX, APX Me-His, and APX Me-His W41F variants were diluted to 1 nM, and 100 μM H$_2$O$_2$ was added to initiate the reaction. Product formation was monitored at 290 nm over 5 min at 25 °C and calculated using ε_{290} = 2.8 mM^{-1} cm^{-1}.[47] All reactions were performed in triplicate to produce a mean rate calculated as moles of substrate oxidized per mol APX per second. These data were plotted against the relevant substrate concentration and fitted using the Michaelis−Menten hyperbolic or Hill functions within Origin software (see Figure S9).

Redox Potentiometry. Optically transparent thin layer electrochemistry (OTTLE) techniques were used to determine the CcP heme redox potentials.[48,49] Briefly, the proteins were exchanged into 100 mM KCl, 50 mM potassium phosphate, 10% glycerol, pH 6, and the following redox mediators were added to ensure efficient equilibration in the electrochemical cell: 20 μM anthraquinone-2-sulfonate, 20 μM phenazine, 25 μM 2-hydroxy-1,4-naphthoquinone, and 6 μM indigotrisulfonate. The solution containing protein and mediators was added to a custom-built OTTLE cell constructed from a flat quartz EPR cell (Wilmad, USA) calibrated against cytc, a platinum gauze working electrode, platinum counter electrode, and an Ag/AgCl reference electrode (BASi, USA). Potentials were applied for 30 min each across the cell using a Biologic SP-150 potentiostat, and titrations were carried out in both reductive and oxidative directions to ensure good equilibration. UV−vis spectra were acquired at each potential using an Agilent Cary

60 UV-visible spectrometer. Heme redox potential was determined by plotting the absorbance at 439 nm (corresponding to the ferrous heme Soret band) against the applied potential and fitting to a standard one-electron Nernst function: $f(x) = (A + B \times 10^{((E_m - x)/59)})/(1 + 10^{((E_m - x)/59)})$, where A and B are the y-axis values representing 0 and 100% reduced CcP, respectively. E_m corresponds to the heme reduction potential. Once it was established that the E_m for both reductive and oxidative titrations was the same, the data was combined and plotted as proportion reduced versus applied potential (vs NHE) and then fitted to the equation above.

Electron Paramagnetic Resonance (EPR) Analysis. Continuous wave EPR spectra were recorded at X-band (~9.4 GHz) using a Bruker ELEXSYS E500/E580 EPR spectrometer (Bruker GmbH, Rheinstetten, Germany). Temperature was maintained using an Oxford Instruments ESR900 helium flow cryostat coupled to an ITC 503 controller from the same manufacturer. EPR sample tubes were 4 mm Suprasil quartz supplied by Wilmad (Vineland, NJ). Compound I was formed using 200 μM protein with 180 μM H$_2$O$_2$ in 50 mM KPi, pH 6 buffer. EPR experiments employed 10 μW microwave power (nonsaturating), 100 kHz modulation frequency, and 1 G (0.1 mT) modulation amplitude to avoid diminution of any partially resolved hyperfine coupling. The experimental temperatures were as given in the text and figure captions.

Stopped-Flow Kinetics. Stopped-flow absorbance experiments were performed on an Applied Photophysics SX18 stopped-flow spectrophotometer (Applied Photophysics Ltd., Leatherhead, UK) equipped with a xenon arc lamp and a 1 cm path length in 50 mM KPi, pH 6 buffer. To follow the spectra evolution of CcP and CcP Me-His ferric or ferrous to compound I and compound II intermediates, respectively, the drive syringes were loaded with separate solutions of 16 μM ferric or ferrous protein (reduced with minimum dithionite) and stoichiometric or 64 μM H$_2$O$_2$.[50] Multiple wavelength data were collected at RT using a (PDA) detector and XSCAN software (see Figure S6).

Second-order rate constants for formation of CcP and CcP Me-His compound I were derived as follows. The drive syringes of the stopped-flow were loaded with separate solutions of 4 μM ferric protein and 16, 24, 32, and 40 μM H$_2$O$_2$. Compound I formation was monitored by an increase in absorbance at 425 nm at 4 °C. Values are an average of three individual measurements (fitted values are given in the Figure S7i), and a linear fit of k_{obs} versus [H$_2$O$_2$] was used to derive a bimolecular rate constant (k_1).

Second-order rate constants for CcP and CcP Me-His compound I reduction were determined in double mixing stopped-flow experiments using an excess of compound I (over cyt$c$) to avoid subsequent reduction of compound II. CcP/CcP Me-His (16 μM) was mixed (1:1) with H$_2$O$_2$ (32 μM) and aged for 1 s to allow complete compound I formation. Cyt$c$II (3 μM) was mixed (1:1) with compound I. Oxidation of ferrous cyt$c$ to the ferric state was monitored by a reduction in absorbance at 550 nm. Consistent with previous studies, determination of k_2 under pseudo-first-order conditions was not possible due to the rapid nature of this electron transfer process.[24,51] The compound I reduction reaction was kinetically modeled by the equation in Figure S7k. Fitting was performed using Mathematica 11 (Wolfram Research Inc.) using the NDSolve and Findfit functions. The time evolution

of [cyt$c$II] was fitted by $A(t) = A_0 + \Delta\varepsilon_{app} \times [\text{cyt}c](t)$. There are three fitting parameters: k, the apparent intrinsic rate constant, described by the ODEs; $\Delta\varepsilon_{app}$ the apparent extinction coefficient difference between the reactant and products; and A_0 the background sample absorbance. Experiments were measured under a single set of conditions with [CcP] = 4 μM, [H$_2$O$_2$] = 8 μM, and [cyt$c$II] = 1.5 μM. The model assumes [compound I] = 4 μM at t_0, that is, all CcP is converted to compound I prior to the second stopped-flow push at t_0 (the conversion to compound I was shown to be complete within 0.2 s in single mixing experiments under comparable conditions). Each experiment was performed in triplicate, and fitted values are given in Figure S7l. Second-order rate constants for CcP and CcP Me-His compound II reduction were determined in double mixing stopped-flow experiments. CcP His/CcP Me-His (6.8 μM) was mixed (1:1) with 6 μM H$_2$O$_2$ and aged for 1 s to allow complete compound I formation. Compound I (3 μM) was subsequently mixed (1:1) with 30, 40, 50, and 70 μM cyt$c$II. Oxidation of ferrous cyt$c$ to the ferric state was monitored by a reduction in absorbance at 550 nm (Figure S7e). Values reported are an average of two to five individual measurements, and all data were fitted to $A_{550} = A_0 + \Delta A(e^{-k_2[\text{cyt}c]_0 t} + e^{-k_{obs}t})$ with k_2 fixed to the value determined above (fitted values are given in Figure S7j). A linear fit of k_{obs} versus [cyt$c$] was used to derive a bimolecular rate constant (k_3).

Solvent Kinetic Isotope Effects and pH Profiling. KSIE and pH profile experiments were performed in a three-component buffer system (37.5 mM acetic acid, 37.5 mM MES, and 75 mM Tris)[52,53] with virtually constant ionic strength over a large pH range (4.00−7.50). Deuterated buffers were prepared in 99.9% D$_2$O, and pD (pH in D$_2$O) was adjusted according to the following relationship: pD = pH$_{obs}$ + 0.38. Buffers were prepared at the following pH/pD values: 4.50, 4.75, 5.00, 5.25, 5.50, 5.75, 6.00, 6.25, 6.50, and 6.75. Concentrated stock solutions of cyt$c$ and H$_2$O$_2$ were prepared in H$_2$O and D$_2$O at pH/pD 6.0 and were used for all assays. Concentrated stock solutions of CcP His and CcP Me-His solutions were prepared in a 50:50 mixture of H$_2$O (pH 6.0) and D$_2$O (pD 6.0) and were used for all assays. For pH profiling, assays were performed at a fixed concentration of cyt$c$ (70 μM). Initial velocities at each pH/pD were determined as described above (see Steady-State Enzyme Kinetic Assays) using the following assay components: 940 μL of appropriate buffer, 10 μL of enzyme (1 nM for CcP His and 10 nM for CcP Me-His), 25 μL of cyt$c$ (70 μM), and 25 μM H$_2$O$_2$ (100 μM). The pH was recorded after each measurement. Reported values are corrected for background cyt$c$ oxidation in the absence of enzyme at the appropriate pH.

For KSIE at pH/pD 5.0 (37.5 mM acetic acid, 37.5 mM MES, and 75 mM Tris) and pH/pD 6.0 (50 mM KPi), steady-state reactions were performed in triplicate to produce a mean rate calculated as moles of cyt$c$II oxidized per mol CcP per second. These data were plotted against the relevant cyt$c$II concentration and fitted using the Michaelis−Menten hyperbolic function within Origin software (see Figure S9).

■ ASSOCIATED CONTENT

ⓢ Supporting Information

The Supporting Information is available free of charge at https://pubs.acs.org/doi/10.1021/acscatal.9b05129.

MS data, UV−vis spectral data, redox potentiometry, kinetic analysis, and structure statistics (PDF)

AUTHOR INFORMATION

Corresponding Author

Anthony P. Green − *Manchester Institute of Biotechnology, School of Chemistry, University of Manchester, Manchester M1 7DN, U.K.;* ● orcid.org/0000-0003-0454-1798; Email: anthony.green@manchester.ac.uk

Authors

Mary Ortmayer − *Manchester Institute of Biotechnology, School of Chemistry, University of Manchester, Manchester M1 7DN, U.K.*

Karl Fisher − *Manchester Institute of Biotechnology, School of Chemistry, University of Manchester, Manchester M1 7DN, U.K.*

Jaswir Basran − *Department of Molecular and Cell Biology and Leicester Institute of Structural and Chemical Biology, Henry Wellcome Building, University of Leicester, Leicester LE1 7RH, U.K.*

Emmanuel M. Wolde-Michael − *Manchester Institute of Biotechnology, School of Chemistry, University of Manchester, Manchester M1 7DN, U.K.*

Derren J. Heyes − *Manchester Institute of Biotechnology, School of Chemistry, University of Manchester, Manchester M1 7DN, U.K.*

Colin Levy − *Manchester Institute of Biotechnology, School of Chemistry, University of Manchester, Manchester M1 7DN, U.K.*

Sarah L. Lovelock − *Manchester Institute of Biotechnology, School of Chemistry, University of Manchester, Manchester M1 7DN, U.K.;* ● orcid.org/0000-0002-4584-3189

J. L. Ross Anderson − *School of Biochemistry, University of Bristol, Bristol BS8 1TD, U.K.;* ● orcid.org/0000-0002-6796-0482

Emma L. Raven − *School of Chemistry, Bristol BS8 1TS, U.K.;* ● orcid.org/0000-0002-1643-8694

Sam Hay − *Manchester Institute of Biotechnology, School of Chemistry, University of Manchester, Manchester M1 7DN, U.K.;* ● orcid.org/0000-0003-3274-0938

Stephen E. J. Rigby − *Manchester Institute of Biotechnology, School of Chemistry, University of Manchester, Manchester M1 7DN, U.K.*

Complete contact information is available at:
https://pubs.acs.org/10.1021/acscatal.9b05129

Notes

The authors declare no competing financial interest.
The crystal structure of CcP Me-His was deposited in the RCSB Protein Data Bank (PDB) under accession number 6H08.

REFERENCES

(1) Poulos, T. L. Heme Enzyme Structure and Function. *Chem. Rev.* **2014**, *114*, 3919−3962.

(2) Huang, X.; Groves, J. T. Oxygen Activation and Radical Transformations in Heme Proteins and Metalloporphyrins. *Chem. Rev.* **2017**, *118*, 2491−2553.

(3) Green, M. T.; Dawson, J. H.; Gray, H. B. Oxoiron(IV) in Chloroperoxidase Compound II is Basic: Implications for P450 Chemistry. *Science* **2004**, *304*, 1653−1656.

(4) Rittle, J.; Green, M. T. Cytochrome P450 Compound I: Capture, Characterization, and C-H Bond Activation Kinetics. *Science* **2010**, *330*, 933−937.

(5) Yosca, T. H.; Rittle, J.; Krest, C. M.; Onderko, E. L.; Silakov, A.; Calixto, J. C.; Behan, R. K.; Green, M. T. Iron(IV)hydroxide pK(a) and the Role of Thiolate Ligation in C-H Bond Activation by Cytochrome P450. *Science* **2013**, *342*, 825−829.

(6) Krest, C. M.; Silakov, A.; Rittle, J.; Yosca, T. H.; Onderko, E. L.; Calixto, J. C.; Green, M. T. Significantly Shorter Fe−S Bond in Cytochrome P450-I is Consistent with Greater Reactivity Relative to Chloroperoxidase. *Nat. Chem.* **2015**, *7*, 696−702.

(7) Wang, X.; Ullrich, R.; Hofrichter, M.; Groves, J. T. Heme-Thiolate Ferryl of Aromatic Peroxygenase is Basic and Reactive. *Proc. Natl. Acad. Sci. U. S. A.* **2015**, *112*, 3686−3691.

(8) Moody, P. C. E.; Raven, E. L. The Nature and Reactivity of Ferryl Heme in Compounds I and II. *Acc. Chem. Res.* **2018**, *51*, 427−435.

(9) Bonagura, C. A.; Bhaskar, B.; Shimizu, H.; Li, H.; Sundaramoorthy, M.; McRee, D. E.; Goodin, D. B.; Poulos, T. L. High-Resolution Crystal Structures and Spectroscopy of Native and Compound I Cytochrome c Peroxidase. *Biochemistry* **2003**, *42*, 5600−5608.

(10) Goodin, D. B.; McRee, D. E. The Asp-His-iron Triad of Cytochrome c Peroxidase Controls the Reduction Potential, Electronic Structure, and Coupling of the Tryptophan Free Radical to the Heme. *Biochemistry* **1993**, *32*, 3313−3324.

(11) de Visser, S. P.; Shaik, S.; Sharma, P. K.; Kumar, D.; Thiel, W. Active Species of Horseradish Peroxidase (HRP) and Cytochrome P450: Two Electronic Chameleons. *J. Am. Chem. Soc.* **2003**, *125*, 15779−15788.

(12) Auclair, K.; Moënne-Loccoz, P.; de Montellano, P. R. O. Roles of the Proximal Heme Thiolate Ligand in Cytochrome P450cam. *J. Am. Chem. Soc.* **2001**, *123*, 4877−4885.

(13) McRee, D. E.; Jensen, G. M.; Fitzgerald, M. M.; Siegel, H. A.; Goodin, D. B. Construction of a Bisaquo Heme Enzyme and Binding by Exogenous Ligands. *Proc. Natl. Acad. Sci. U. S. A.* **1994**, *91*, 12847−12851.

(14) Hirst, J.; Wilcox, S. K.; Ai, J.; Moënne-Loccoz, P.; Loehr, T. M.; Goodin, D. B. Replacement of the Axial Histidine Ligand with Imidazole in Cytochrome c Peroxidase. 2. Effects on Heme Coordination and Function. *Biochemistry* **2001**, *40*, 1274−1283.

(15) Takahashi, A.; Kurahashi, T.; Fujii, H. Effect of Imidazole and Phenolate Axial Ligands on the Electronic Structure and Reactivity of Oxoiron(IV) Porphyrin π-Cation Radical Complexes: Drastic Increase in Oxo-Transfer and Hydrogen Abstraction Reactivities. *Inorg. Chem.* **2009**, *48*, 2614−2625.

(16) Sivaraja, M.; Goodin, D. B.; Smith, M.; Hoffman, B. M. Identification by ENDOR of Trp191 as the Free-Radical Site in Cytochrome c Peroxidase Compound ES. *Science* **1989**, *245*, 738−740.

(17) Chreifi, G.; Baxter, E. L.; Doukov, T.; Cohen, A. E.; McPhillips, S. E.; Song, J.; Meharenna, Y. T.; Soltis, S. M.; Poulos, T. L. Crystal Structure of the Pristine Peroxidase Ferryl Center and its Relevance to Proton-Coupled Electron Transfer. *Proc. Natl. Acad. Sci. U. S. A.* **2016**, *113*, 1226−1231.

(18) Casadei, C. M.; Gumiero, A.; Metcalfe, C. L.; Murphy, E. J.; Basran, J.; Concilio, M. G.; Teixeira, S. C. M.; Schrader, T. E.; Fielding, A. J.; Ostermann, A.; Blakeley, M. P.; Raven, E. L.; Moody, P. C. E. Neutron Cryo-Crystallography Captures the Protonation State of Ferryl Heme in a Peroxidase. *Science* **2014**, *345*, 193−197.

(19) Xiao, H.; Peters, F. B.; Yang, P. Y.; Reed, S.; Chittuluru, J. R.; Schultz, P. G. Genetic Incorporation of Histidine Derivatives Using an Engineered Pyrrolysyl-tRNA Synthetase. *ACS Chem. Biol.* **2014**, *9*, 1092−1096.

(20) Wang, J.; Mauro, J. M.; Edwards, S. L.; Oatley, S. J.; Fishel, L. A.; Ashford, V. A.; Xuong, N. H.; Kraut, J. X-ray structures of recombinant yeast cytochrome c peroxidase and three heme-cleft mutants prepared by site-directed mutagenesis. *Biochemistry* **1990**, *29*, 7160−7173.

(21) Houseman, A. L. P.; Doan, P. E.; Goodwin, D. B.; Hoffman, B. M. Comprehensive explanation of the anomalous EPR spectra of wild-type and mutant cytochrome c peroxidase compound ES. *Biochemistry* **1993**, *32*, 4430−4443.

(22) Miner, K. D.; Pfister, T. D.; Hosseinzadeh, P.; Karaduman, N.; Donald, L. J.; Loewen, P. C.; Lu, Y.; Ivancich, A. Identifying the Elusive Sites of Tyrosyl Radicals in Cytochrome c Peroxidase: Implications for Oxidation of Substrates Bound at a Site Remote from the Heme. *Biochemistry* **2014**, *53*, 3781−3789.

(23) Ivancich, A.; Dorlet, P.; Goodin, D. B.; Un, S. Multifrequency High-Field EPR Study of the Tryptophanyl and Tyrosyl Radical Intermediates in Wild-Type and the W191G Mutant of Cytochrome c Peroxidase. *J. Am. Chem. Soc.* **2001**, *123*, 5050−5058.

(24) Hahm, S.; Miller, M. A.; Geren, L.; Kraut, J.; Durham, B.; Millett, F. Reaction of Horse Cytochrome c with the Radical and the Oxyferryl Heme in Cytochrome c Peroxidase Compound I. *Biochemistry* **1994**, *33*, 1473−1480.

(25) Efimov, I.; Badyal, S. K.; Metcalfe, C. L.; Macdonald, I.; Gumiero, A.; Raven, E. L.; Moody, P. C. E. Proton Delivery to Ferryl Heme in a Heme Peroxidase: Enzymatic Use of the Grotthuss Mechanism. *J. Am. Chem. Soc.* **2011**, *133*, 15376−15383.

(26) Gray, H. B.; Winkler, J. R. Living with Oxygen. *Acc. Chem. Res.* **2018**, *51*, 1850−1857.

(27) Goodin, D. B.; Davidson, M. G.; Roe, J. A.; Mauk, A. G.; Smith, M. Amino acid substitutions at tryptophan-51 of cytochrome c peroxidase: effects on coordination, species preference for cytochrome c, and electron transfer. *Biochemistry* **1991**, *30*, 4953−4962.

(28) Pfister, T. D.; Gengenbach, A. J.; Syn, S.; Lu, Y. The Role of Redox-Active Amino Acids on Compound I Stability, Substrate Oxidation, and Protein Cross-Linking in Yeast Cytochrome c Peroxidase. *Biochemistry* **2001**, *40*, 14942−14951.

(29) Green, A. P.; Hayashi, T.; Mittl, P. R. E.; Hilvert, D. A Chemically Programmed Proximal Ligand Enhances the Catalytic Properties of a Heme Enzyme. *J. Am. Chem. Soc.* **2016**, *138*, 11344−11352.

(30) Lad, L.; Mewies, M.; Raven, E. L. Substrate Binding and Catalytic Mechanism in Ascorbate Peroxidase: Evidence for Two Ascorbate Binding Sites. *Biochemistry* **2002**, *41*, 13774−13781.

(31) Sharp, K. H.; Mewies, M.; Moody, P. C. E.; Raven, E. L. Crystal Structure of the Ascorbate Peroxidase-Ascorbate Complex. *Nat. Struct. Biol.* **2003**, *10*, 303−307.

(32) Hayashi, T.; Hilvert, D.; Green, A. P. Engineered Metal-loenzymes with Non-Canonical Coordination Environments. *Chem. − Eur. J.* **2018**, *24*, 11821−11830.

(33) Aldag, C.; Gromov, I. A.; García-Rubio, I.; von Koenig, K.; Schlichting, I.; Jaun, B.; Hilvert, D. Probing the Role of the Proximal Heme Ligand in Cytochrome P450cam by Recombinant Incorpo-ration of Selenocysteine. *Proc. Natl. Acad. Sci. U. S. A.* **2009**, *106*, 5481−5486.

(34) Sivaramakrishnan, S.; Ouellet, H.; Matsumura, H.; Guan, S.; Moënne-Loccoz, P.; Burlingame, A. L.; Ortiz de Montellano, P. R. Proximal Ligand Electron Donation and Reactivity of the Cytochrome P450 Ferric−Peroxo anion. *J. Am. Chem. Soc.* **2012**, *134*, 6673−6684.

(35) Onderko, E. L.; Silakov, A.; Yosca, T. H.; Green, M. T. Characterization of a Selenocysteine-Ligated P450 Compound I Reveals Direct Link Between Electron Donation and Reactivity. *Nat. Chem.* **2017**, *9*, 623−628.

(36) Pott, M.; Hayashi, T.; Mori, T.; Mittl, P. R. E.; Green, A. P.; Hilvert, D. A Noncanonical Proximal Heme Ligand Affords an Efficient Peroxidase in a Globin Fold. *J. Am. Chem. Soc.* **2018**, *140*, 1535−1543.

(37) Choudhury, K.; Sundaramoorthy, M.; Hickman, A.; Yonetani, T.; Woehl, E.; Dunn, M. F.; Poulos, T. L. Role of the Proximal Ligand in Peroxidase Catalysis. Crystallographic, Kinetic, and Spectral Studies of Cytochrome c Peroxidase Proximal Ligand Mutants. *J. Biol. Chem.* **1994**, *269*, 20239−20249.

(38) Nonaka, D.; Wariishi, H.; Welinder, K. G.; Fujii, H. Paramagnetic ^{13}C and ^{15}N NMR Analyses of the Push and Pull Effects in Cytochrome c Peroxidase and Coprinus cinereus Peroxidase Variants: Functional Roles of Highly Conserved Amino Acids around Heme. *Biochemistry* **2010**, *49*, 49−57.

(39) Roe, J. A.; Goodin, D. B. Enhanced Oxidation of Aniline Derivatives by Two Mutants of Cytochrome c Peroxidase at Tryptophan 51. *J. Biol. Chem.* **1993**, *268*, 20037−20045.

(40) Knapp, M. J.; Rickert, K.; Klinman, J. P. Temperature-Dependent Isotope Effects in Soybean Lipoxygenase-1: Correlating Hydrogen Tunneling with Protein Dynamics. *J. Am. Chem. Soc.* **2002**, *124*, 3865−3874.

(41) Mitchell, A. J.; Zhu, Q.; Maggiolo, A. O.; Ananth, N. R.; Hillwig, M. L.; Liu, X.; Boal, A. K. Structural Basis for Halogenation by Iron- and 2-Oxo-Glutarate Dependent Enzyme WelO5. *Nat. Chem. Biol.* **2016**, *12*, 636−640.

(42) Kan, S. B. J.; Huang, X.; Gumulya, Y.; Chen, K.; Arnold, F. H. Genetically Programmed Chiral Organoborane Synthesis. *Nature* **2017**, *552*, 132−136.

(43) Gumiero, A.; Metcalfe, C. L.; Pearson, A. R.; Raven, E. L.; Moody, P. C. E. Nature of the Ferryl Heme in Compounds I and II. *J. Biol. Chem.* **2011**, *286*, 1260−1268.

(44) Lam, S. S.; Martell, J. D.; Kamer, K. J.; Deerinck, T. J.; Ellisman, M. H.; Mootha, V. K.; Ting, A. Y. Directed Evolution of APEX2 for Electron Microscopy and Proximity Labeling. *Nat. Methods* **2015**, *12*, 51−54.

(45) McCoy, A. J.; Grosse-Kunstleve, R. W.; Adams, P. D.; Winn, M. D.; Storoni, L. C.; Read, R. J. Phaser Crystallographic Software. *J. Appl. Cryst.* **2007**, *40*, 658−674.

(46) Kang, D. S.; Erman, E. J. The Cytochrome c Peroxidase-Catalyzed Oxidation of Ferrocytochrome c by Hydrogen Peroxide. Steady State Kinetic Mechanism. *J. Bio. Chem.* **1982**, *257*, 12775−12779.

(47) Murphy, E. J.; Metcalfe, C. L.; Basran, J.; Moody, P. C. E.; Raven, E. L. Engineering the Substrate Specificity and Reactivity of a Heme Protein: Creation of an Ascorbate Binding Site in Cytochrome c Peroxidase. *Biochemistry* **2008**, *47*, 13933−13941.

(48) Ost, T. W. B.; Clark, J. P.; Anderson, J. L. R.; Yellowlees, L. J.; Daff, S.; Chapman, S. K. 4-Cyanopyridine, a Versatile Spectroscopic Probe for Cytochrome P450 BM3. *J. Biol. Chem.* **2004**, *279*, 48876−48882.

(49) Watkins, D. W.; Jenkins, J. M. X.; Grayson, K. J.; Wood, N.; Steventon, J. W.; Le Vay, K. K.; Goodwin, M. I.; Mullen, A. S.; Bailey, H. J.; Crump, M. P.; MacMillan, F.; Mulholland, A. J.; Cameron, G.; Sessions, R. B.; Mann, S.; Anderson, J. L. R. Construction and In Vivo Assembly of a Catalytically Proficient and Hyperthermostable De Novo Enzyme. *Nat. Commun.* **2017**, *8*, 358.

(50) Ho, P. S.; Hoffman, B. M.; Kang, C. H.; Margoliash, E. Control of the Transfer of Oxidizing Equivalents between Haem Iron and Free Radical Site in Yeast Cytochrome c Peroxidase. *J. Biol. Chem.* **1983**, *258*, 4356−4363.

(51) Chreifi, G.; Hollingsworth, S. A.; Li, H.; Tripathi, S.; Arce, A. P.; Magaña-Garcia, H. I.; Poulos, T. L. Enzymatic Mechanism of Leishmania major Peroxidase and the Critical Role of Specific Ionic Interactions. *Biochemistry* **2015**, *54*, 3328−3336.

(52) Mauro, J. M.; Fishel, L. A.; Hazzard, J. T.; Meyer, T. E.; Tollin, G.; Cusanovich, M. A.; Kraut, J. Tryptophan-191 .fwdarw. phenylalanine, a proximal-side mutation in yeast cytochrome c peroxidase that strongly affects the kinetics of ferrocytochrome c oxidation. *Biochemistry* **1988**, *27*, 6243−6256.

(53) Ellis, K. J.; Morrison, J. F. Buffers of constant ionic strength for studying pH-dependent processes. *Methods Enzymol.* **1982**, *87*, 405−426.